Proceedings World Geothermal Congress 2020+1
Reykjavik, Iceland, April - October 2021

Geological Characteristics and Geothermal Genesis of Deep Granite Geothermal Reservoir in Southeast Coastal Areas in China

Herong ZHENG, Zongquan HU, Jun LUO, Ying Zhang, Jianyun Feng, Yan Zeng

Sinopec Petroleum Exploration and Production Research Institute, No. 5, Baisha Road, Changping District, Beijing, China

luojun.syky@sinopec.com

Keywords: southeast coastal areas, granite geothermal reservoir, geothermal resources

ABSTRACT

The southeast coastal areas in China have distributed lots of granite outcrops of different periods. Previous research has shown that granites are also distributed under sedimentary basins in these areas. Therefore, granites with fractures buried in deep can be used as a potential deep geothermal reservoir in these areas. In order to study geological conditions of the deep granite reservoir and establish the genesis model of the deep granite geothermal system, rock geochemistry and zircon U-Pb chronology from outcrop and parts of the drilling cores of granitic rocks have been analyzed, combined with the anatomy of the deep seismic data. Based on the results of geochemistry and zircon U-Pb chronology, most granites in this area are of Yanshanian periods. The formation background of granites is the advance and retraction of westward subduction of Pacific plate. According to the seismic data, the thickness of the overlying strata on granite in Huangshadong area of Huizhou City is up to 1.5 km. According to the regional geological survey, multi-stage joints are developed in the granite, and a large number of hot springs rise to the surface. The heat source in the study area mainly comes from the mantle carried up by the deep NNE-trending faults. There are a large number of thermal springs at the intersection of the surface and the NW-trending fault, and the NW-trending fault provides the drainage conditions for the upwelling of underground thermal springs. There is a huge amount of deep granite geothermal resources in the southeast coastal area. The analysis of deep granite geological conditions and genetic models can provide guidance for the evaluation of deep granite geothermal resources and the further optimization of favorable zones in these areas.

1. INTRODUCTION

Geothermal resources, as a renewable and clean energy, have been widely used globally in recent years, and the utilization has been increasing year by year (Bertani, 2012, 2016; Lund and Boyd, 2016). Most of the geothermal resources under exploitation and utilization are hydrothermal geothermal resource, which is widely distributed (Li Dewei and Wang Yanxin, 2015). Deep geothermal resources are considered as an important part of future energy supply due to their huge thermal energy storage and reserves. Most of the deep geothermal exploration and experimental base is granite (Brown et al., 2012), and numerous studies have shown that the granite radioactive heat production has significant contribution to the heat source, such as Australia Cooper basin geothermal field caused by granites with intrusion age less than 0.5 Ma (Goldstein et al., 2008), Rose-manowes geothermal field in England due to Early Permian granite heat generation (Richards et al., 1992), the Soultz geothermal field in France due to Late Paleozoic granite heat generation (Genter et al., 1995).

Granite is widely distributed in the southeast coastal area of China, with an outcropping area of 20,000 km^2, accounting for about 1/5 of the area, and it is considered to be formed in three phases, i.e. Caledonian, Indosinian and Yanshanian period (Zhou et al., 2006) (Figure 1). Radioactive elements from granites such as rich in U, Th, K, are important radioactive elements to generate heat by atom decaying. The ideal place with covering layer, may obtain the ideal granite geothermal reservoir. Meanwhile, Southeast coastal areas in China is the second largest region with high heat flow value (Hu et al., 2000). Xi et al. (2018) analyzed the gravity anomaly in Guangdong province and concluded that the decay of thermal elements in granite may be an important part of the geothermal heat sources in the southeast coastal areas. The region is rich in geothermal resources, covering medium-low temperature, medium-high temperature and high-temperature geothermal resources.

In order to further study geological conditions of the deep granite reservoir and establish the genesis model of the deep granite geothermal system, this paper has adopted rock samples from outcrop and parts of the drilling core rocks to analyze the formation background of granite and its geothermal significance to the southeast region in China.

2. GEOLOGICAL SETTING

The outcropping stratigraphic units in the Southeast coastal areas are similar to those in the Cathaysia block (Wang et al., 2013), including pre-Cambrian, Cambrian, Ordovician, Devonian, Carboniferous, Permian, Triassic, Jurassic, Cretaceous, Paleogene and Quaternary strata. The area has experienced multiple periods of intense magmatic events since the Paleozoic, mainly manifested as a large number of Paleozoic and Mesozoic granitic rocks (Wang et al., 2013) (Figure 2) and Cenozoic mafic magmatism (Gong and John, 2014). Large-scale structural deformation caused by emplacements are very strong to the stratum reconstruction, forming a series of faults of different scales and different properties, with the northeast, northwest and east-west direction.

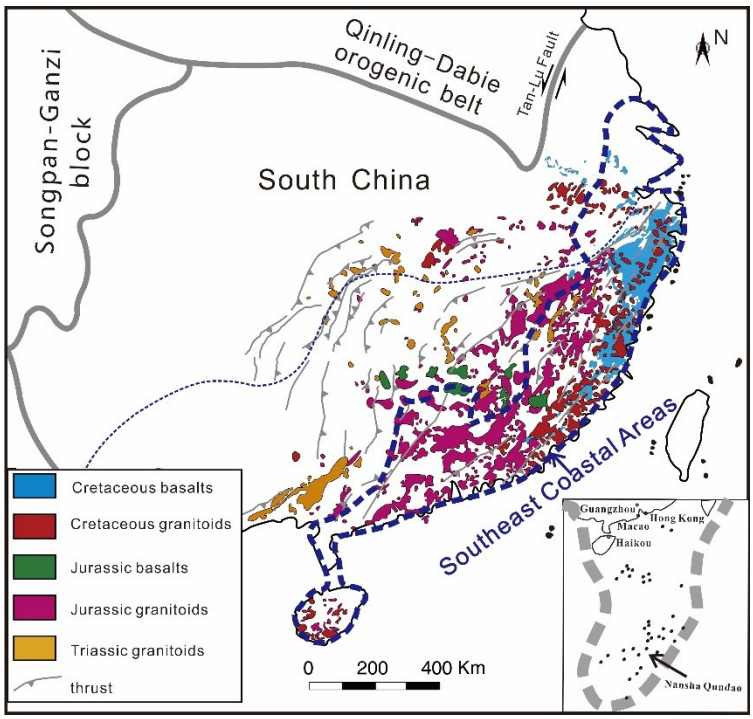

Figure 1: The granite distribution map of the study area

The distribution of most granite geothermal fields is mainly controlled by the deep and large fault in NE direction, and most of them are beaded along the Neo-Cathaysian faults. The zone has experienced many violent tectonic movements and multiple periods of magma intrusion, resulting in secondary faults, rock mass fragmentation and tensile joint fractures near the fault zone, providing space and channels for the storage and migration of geothermal fluids. At the same time, the tectonic activities of deep and large faults not only promote the formation of heat storage space, but also communicate the spatial connection between deep geothermal fluids and shallow geothermal reservoirs, becoming an important heat transfer channel in geothermal fields. From the regional analysis, most of the geothermal fields are linear distribution along the fault zone, mainly exposed on the deep fault axis. The rest are mostly distributed among the deep and large faults, which are locally influenced by the secondary NW tensioned water-conducting faults or pinnate faults.

Favorable granite geothermal reservoir is distributed in the exposed magmatic rock mass, near the late intrusive dike or the contact zone between rock mass and surrounding rock mass. The distribution of geothermal field is not only related to the fracture and fracture development of primary rock mass and contact zone rock due to the multi-stage intrusion of magma or the influence of deep fault structure, but also related to the geological age of intrusive rock.

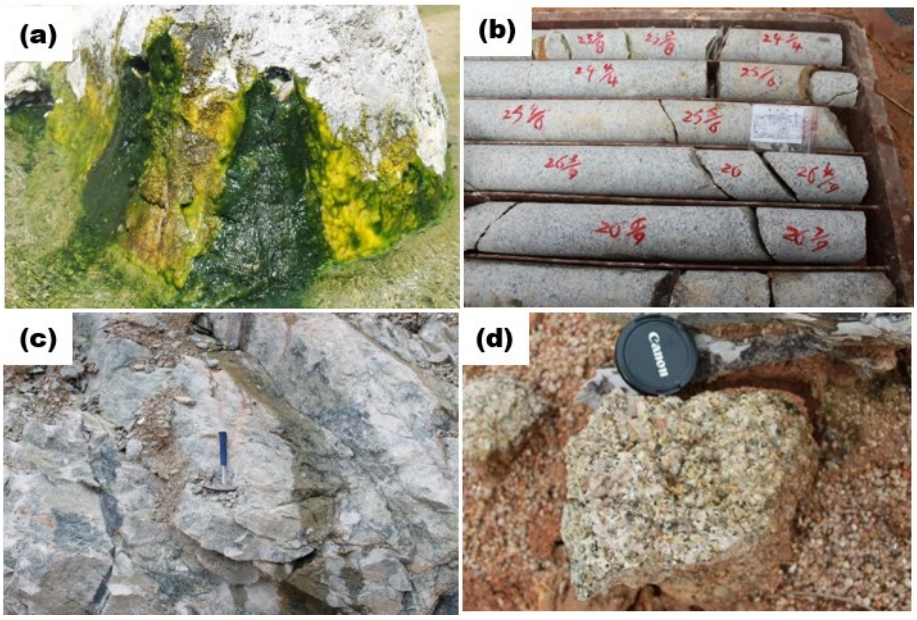

Figure 2: Photograph showing outcrops of granites in different areas

The granite samples collected were mainly distributed along a line of about 1,300 kilometers with an exposed area of about 10 to 784 square kilometers. These granites are mainly granitic, with a few being orthogonality, quartz dimorphism and granitic diorite, with

granular structure of different thickness and fineness (Figure 3). The mineralogy of these samples is relatively simple, consisting mainly of plagioclase (30-42%), potash feldspar (30-8%), quartz (20-30%), biotite (5%), and a small amount of amphibole (2-10%). Accessory minerals include sphene, zircon, and titanium-iron oxides.

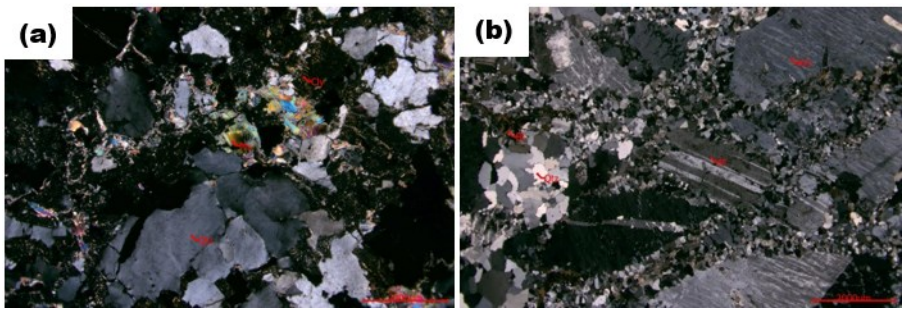

Figure 3: Photomicrographs showing mineral assemblage of representative granites. The abbreviations are: Pl-plagioclase, Qz-quartz, Bt-biotite, Kfs-K-feldspar, Amp-amphibole.

3. ANALITICAL METHODS

In order to interpret magmatism in the study area of granite, a total of 16 samples of magmatic rocks (Figure 1B) were collected in this study and measured by principal trace element analysis, and zircon U-Pb dating analysis was conducted for 4 granite samples.

U-Pb dating and trace element analyses of zircon were conducted synchronously by LA-ICP-MS at the State Key Laboratory of Geological Processes and Mineral Resources, China University of Geosciences, Wuhan. Detailed operating conditions for the laser ablation system and the ICP-MS instrument and data reduction are the same as description by Liu et al. (2010). Laser sampling was performed using a GeoLas 2005. An Agilent 7500a ICP-MS instrument was used to acquire ion-signal intensities. A “wire” signal smoothing device is included in this laser ablation system, by which smooth signals are produced even at very low laser repetition rates down to 1 Hz (Hu et al., 2012b). Helium was applied as a carrier gas. Argon was used as the make-up gas and mixed with the carrier gas via a T-connector before entering the ICP. Nitrogen was added into the central gas flow (Ar+He) of the Ar plasma to decrease the detection limit and improve precision (Hu et al., 2008a; Liu et al., 2010). Each analysis incorporated a background acquisition of approximately 20-30 s (gas blank) followed by 50 s of data acquisition from the sample. The Agilent Chemstation was utilized for the acquisition of each individual analysis. Off-line selection and integration of background and analyze signals, and time-drift correction and quantitative calibration for trace element analyses and U-Pb dating were performed by ICPMS DataCal (Liu et al., 2010).

Zircon 91500 was used as external standard for U-Pb dating, and was analyzed twice every 5 analyses. Time-dependent drifts of U-Th-Pb isotopic ratios were corrected using a linear interpolation (with time) for every five analyses according to the variations of 91500 (i.e., 2 zircon 91500 + 5 samples + 2 zircon 91500) (Liu et al., 2010). Preferred U-Th-Pb isotopic ratios used for 91500 are from Wiedenbeck et al. (1995). Uncertainty of preferred values for the external standard 91500 was propagated to the ultimate results of the samples. Concordia diagrams and weighted mean calculations were made using Isoplot/Exver3 (Ludwig, 2003). Trace element compositions of zircons were calibrated against multiple-reference materials (BCR-2G and BIR-1G) combined with internal standardization (Liu et al., 2010). The preferred values of element concentrations for the USGS reference glasses are from the GeoReM database.

4. RESULTS

4.1 U-Pb dating

CL images of typical zircons of 4 samples, and their concordance ages and analysis results are shown in Figure 4. It can be seen from the CL image that the zircons generally have good autogenesis. Most of them are columnar or long-column-cone shaped with a length of 50~360 m. The aspect ratio of most of them is about 1.5:1~3:1, which is similar to the characteristics of magmatic zircons (Wu Yuanbao and Zheng Yongfei, 2004). The dating results show that the rock mass in the study area has a wide age distribution, ranging from 142.9 to 168 Ma. Among the samples, the age of $^{238}U/^{206}Pb$ rock mass is the highest, and the weighted average age of $^{238}U/^{206}Pb$ rock mass is 168.4±3.5 Ma (MSWD=5.9, N=15), and the age of $^{238}U/^{206}Pb$ rock mass is the lowest, and the weighted average age of $^{238}U/^{206}Pb$ is 142.9±1.4Ma (MSWD=1.3, N=15). There is no obvious pattern of age distribution of such samples in the region. In general, the age of all samples in the study area shows that there are three tectonic thermal events in the area, namely Caledonian, Indosinian and Yanshanian. The Yanshanian tectonic thermal events are the dominant thermal events in the area, and most of the rocks in the area are the products of this thermal event.

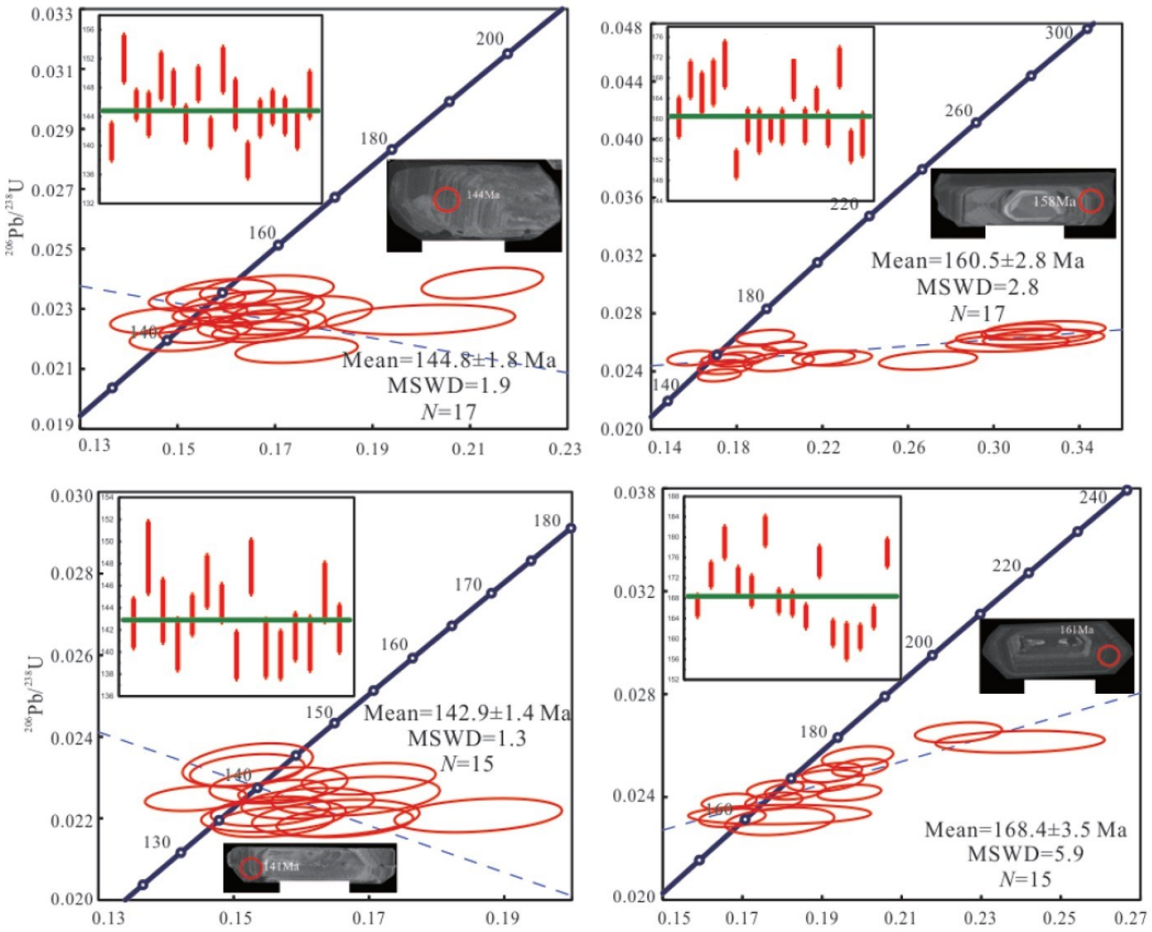

Figure 4: Cathodoluminescence (CL) images of representative zircons and Concordia plots of the granites.

4.2 Geochemistry

Rock geochemical test results show that the rock mass geochemical composition analyses are as follows: SiO_2 content ranged from 63.37% to 76.71% with an average of 73.13%; TiO_2 content ranged from 0.02% to 0.95% with an average of 0.25%; Al_2O_3 content ranged from 11.94% to 15.49% with an average of 13.40%; MgO content ranged from 0.02% to 2.25% with an average of 0.53%; and (K_2O+Na_2O) content ranged from 5.04% to 8.99% with an average of 7.75%.

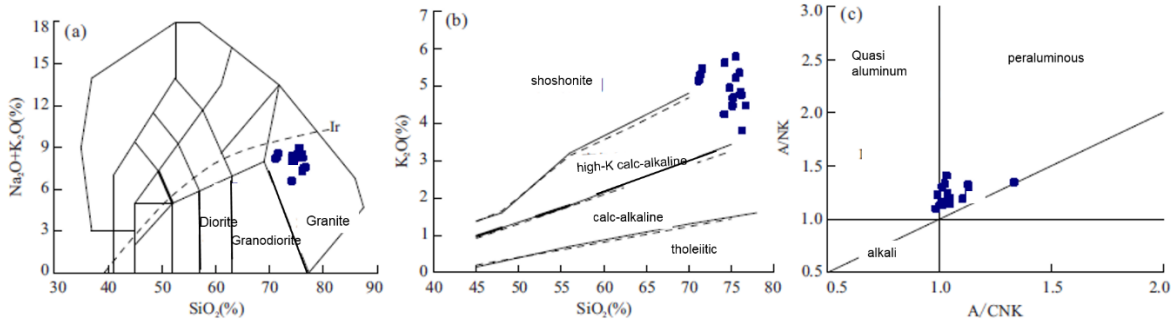

Figure 5: TAS, SiO_2-K_2O and A/CN diagrams of magmatic rocks.

At the diagram of SiO_2 (Na_2O+K_2O) (Figure 5), sample dots fell within the granite region. According to the diagram of SiO_2-K_2O (Figure 5), the contact point of Yanshan period falls within the range of calc-alkaline series, and the rest falls within the range of high potassium calc-alkaline series-potassium basalt series, mainly manifested as high potassium calc-alkaline. The aluminum saturation index (A/CNK) ranges from 0.88 to 1.33 and ranges mainly from 1.0 to 1.1 on the diagram of A/NK –A/CNK (Figure 5).

On the primitive mantle normalized trace element spider diagram (Figure 6), Large Ionic Lithophile Elements (LILE) such as K and Rb, Th and U are enriched, and there is a strong loss of Ba, Sr and High Field Strong Elements (HFSE) such as Nb, Ti, Ta and P, which are similar to the geochemical characteristics of rocks in the subduction zone (Kelemen et al., 2003). On the Chondrite Normalized REE distribution diagram (Figure 6), the pattern is smooth and show light rare earth element (LREE) concentration and heavy rare earth element (HREE) losses. Eu in the pattern shows negative anomaly, indicating that the magma evolution of plagioclase crystallization separation. The value of ΣREE is between 50.50×10^{-6}-401.02×10^{-6}, with a mean of 183.31×10^{-6}. The value of LREE/HREE is 0.84 ~ 12.46, with an average of 6.44, showing that obvious fractionation between light and heavy rare earth. The

value of $(La/Yb)_N$ is 0.67 ~ 19.24, while the average value is 7.18. The value of Eu is between 0.03~0.71, and the average value is 0.32. In primitive mantle normalized trace element spider diagram, most of the sample elements distribution features are similar, indicating that most of the samples have the same or similar formation patterns.

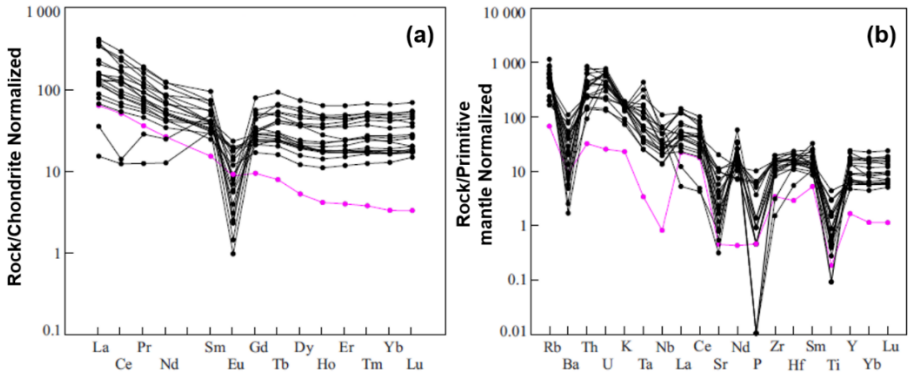

Figure 6: Chondrite Normalized REE distribution patterns (a) and primitive mantle normalized trace element spider diagram (b) of granitic rocks.

It can be seen from diagrams of Rb-Y and Rb-Th (Figure 7) that with the increase of Rb content, Y and Th content increase, which is consistent with the evolutionary trend of typical Type I granite (Lackey et al., 2005). Therefore, the granite in the study area is mainly the high-differentiation I-type granite.

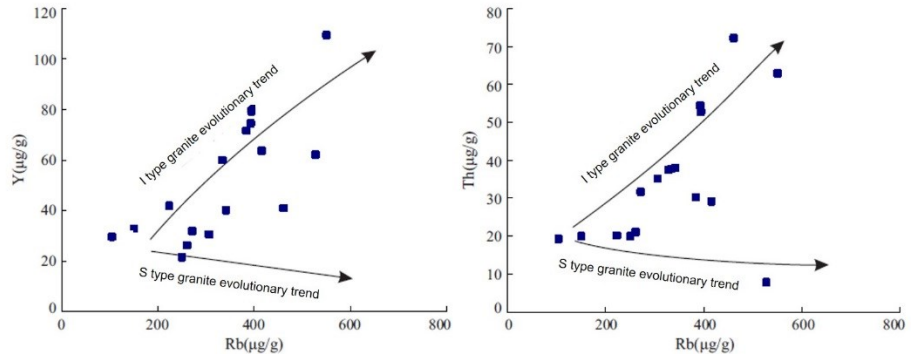

Figure 7: Rb-Y and Rb-Th diagrams of granitic rocks.

5. DISCUSSION

5.1 Genetic mechanism of granite

On the SiO_2 - $FeO_T/(FeO_T + MgO)$ and SiO_2 - Al_2O_3 diagram (Figure 8), most samples are plotted in the POG (post-Orogenic Grabite) zone (Frost et al., 2001). On the Rb + Nb (Y) and (Yb + Ta) - Rb diagram, samples are plotted within the scope of the volcanic island arc granite (VAG), within plate granite (WPG) and sys-collision granite (syn-COLG). Many studies indicate that the Yanshanian granites in Southeast Coastal areas in China was influenced by paleo-pacific plate subduction (Li et al., 2007,2018; Li and Li, 2007; Wang et al., 2013). Although scholars still have disputes on the form of paleo-Pacific plate subduction, it is agreed that the paleo-Pacific plate in the early Yanshanian period was a forward subduction, and the middle-late Yanshanian period was a retractable subduction with extensional environment (Li et al., 2007; Wang et al., 2013). The earliest age of all Yanshanian samples is calc-alkaline quasi-aluminum granodiorite of early and middle Yanshanian, and it is a typical origin of island arc, which is associated with forward subduction of the Paleo-Pacific plate. The other samples are high potassium calcium alkaline granites of middle and late Yanshanian period, which is related to the extensional environment formed by retractable subduction of the ancient Pacific plate. The Yanshanian granite rock mass production in the study area is due to paleo-Pacific plate subduction.

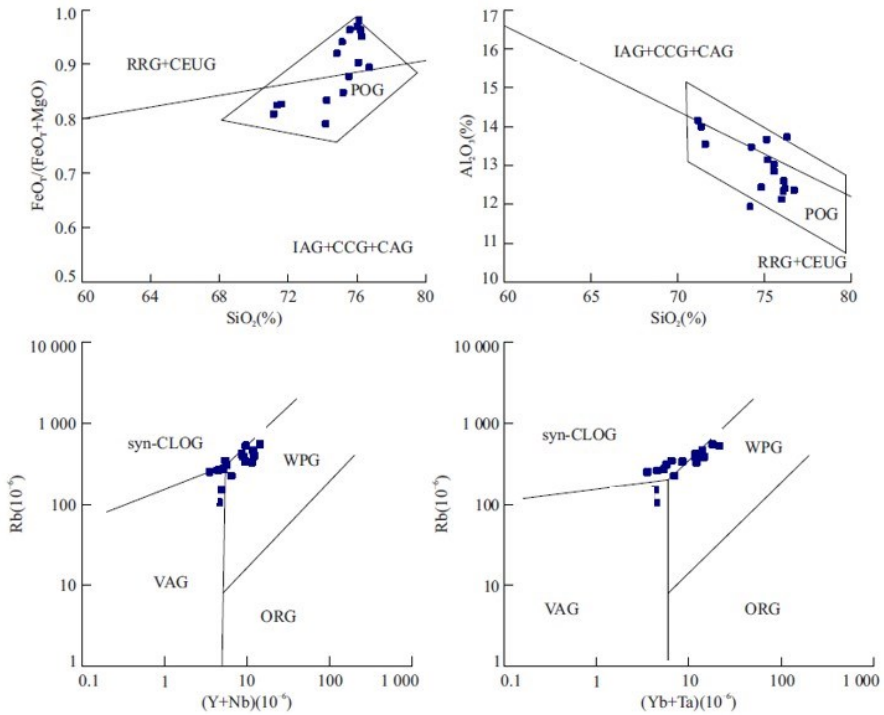

Figure 8: SiO_2-FeO_T/(FeO_T+MgO), SiO_2 - Al_2O_3, (Y+Nb)-Rb and (Yb+Ta)-Rb diagrams of granites

5.2 Discussion on the burial depth of deep granite

5.2.1 Seismic profiles in Huangshadong area of Guangdong Province

The 2 seismic profiles in Huangshadong area of Guangdong Province (Figure 9) (Kuang et al., 2020) reflect the sedimentary strata overlying granites. The sedimentary strata in the study area have undergone complex tectonic evolution, repeated tectonic uplifting, compression folding and fault processes have caused the sedimentary strata to have dramatic occurrence changes in a small range, and multiple periods of magmatic intrusion and eruption have complicated the contact relationship strata and rock mass. Therefore, the spatial continuity of stratigraphic interface and the stability of fault characteristics in seismic profile are poor in different ages.

According to the profiles of seismic inversion (Figure 9), the buried depth of Tg (interface between sedimentary strata and granites) is generally located between 1,000 ~ 1,900 ms (corresponding depth is about 1,400 ~ 2,200 m), and the seismic phase characteristics of Tg interface are significantly different from each other. The granite core sample from Well Huire 1 is similar to Yanshanian granite, indicating that seismic facies unit may correspond to the intrusive body in Yanshanian period, emplaced from the deep crust upward into shallow rock bed. 2050- 2900 ms (corresponding to the depth of about 3600-4800 m) for the bedrock under the bottom of the interface (Td), reflection of geological units in phase axis continuity better, different from the adjacent granite rock mass. It may be older sedimentary rocks or metamorphic rocks with certain stratification.

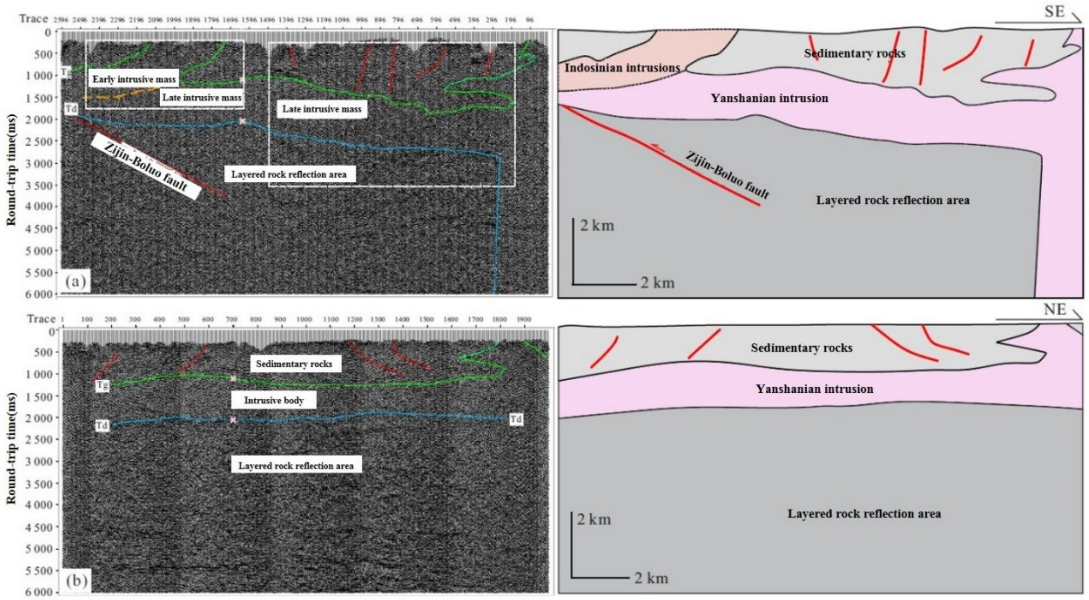

Figure 9: Profiles of seismic inversion and its geological interpretation in Huangshadong area (Kuang et al., 2020)

5.2.2 Apparent resistivity inversion Profiles in North Hainan Province

In the area outside the east of Fushan Depression of Hainan Province, wide field electromagnetic detection has been conducted (Figure 10) (Tan et al., 2019). From the resistivity profile of the final inversion processing, a set of high resistance developed in the west of the L1 line and a set of low resistance developed in the east. The two parts were clearly bounded and featured with great difference. Based on regional geological analysis, the corresponding geological model is established, and it is preliminarily considered that the high resistivity in the east is a set of intrusive concealed granite, and the low resistivity in the west is a paleoproximal sedimentary stratum, and the middle fault controls its scale. According to the analysis of geological model, the basement of North Hainan area is composed of pre-Mesozoic sedimentary rocks and granite intrusive bodies, and the rock strains develop. The fault-block-graben-barrier is developed in this area, and the structure is complex. The fault-block-graben-barrier structure is developed in the east, which is similar to Fushan Depression. Moreover, the distribution of Paleogene strata is obviously controlled by the size of the fault depression. The L4 line extends southward to the granite outflowing area. According to the resistivity result diagram, the electrical characteristics of the outflowing granite are similar to those of the latent granite. By comparing the two survey lines, the latent high-resistivity stability exists. In the intersection area where survey line L1 and survey line L4 meet, the granite has a large scale, a buried depth of about 3000m, and an overburden, which is a potential favorable area for deep high-temperature geothermal exploration.

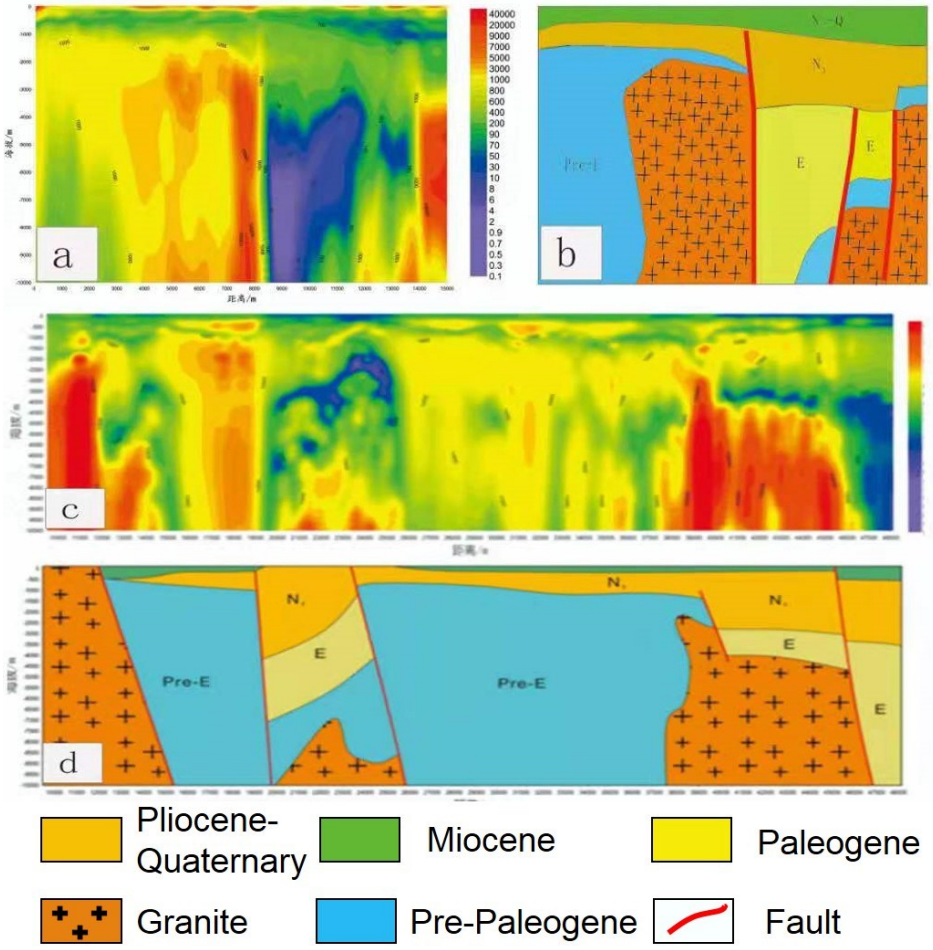

Figure 10: Profiles of apparent resistivity inversion based on wide field electromagnetic method and corresponding geological interpretation in North Hainan Province (Tan et al., 2020)

5.3 The significance of granite to the geothermal energy

The heat source of geothermal energy mainly include heat transfer in the mantle, local anomalous heat transfers in the crust (magma chamber), and radioactive heat generation from granitic rocks. Surface heat flow, as a direct reflection of deep heat, usually accounts for 40%~60% of the heat flow from the mantle. The heat flow caused by radioactive heat generation in the crust is slightly less than that from the mantle, accounting for about 40% and up to 50% in some areas (Wang Shejiao et al., 1999). The terrestrial heat flow value in the study area is about 70 mW/m^2, which is higher than the average terrestrial heat flow value of 64.2mW/m^2 in South China (Yuan et al., 2006). The Yanshannian granite in the Southeast Coastal region has a high thermal conductivity, with an average thermal conductivity of 3.15 W/mK. This means that the granite in the deep part with a thickness of up to 3.5km can better conduct the heat in the deeper part to the near surface. Consequently, the mantle heat gets better performance on the surface, which promotes the formation of the geothermal energy in the area.

Former research suggested that the heat generated by radioactive element decay in rocks is one of the main sources of earth heat (Huang Shaopeng, 1992), and it is also a major factor controlling the temperature field distribution in the lithosphere (Sclater et al., 1980). Existing data also show that there is no magma chamber or mantle thermal anomaly in the region. In addition, previous scholars proposed that the lower crust has little influence on the surface heat flow value (Hasterok and Chapman, 2007), and the research on the lower crust inclusion also shows that the radioactive heat generation rate of rocks in the lower crust is very low (Rudnick and

Fountain, 1995). Thus, the heat source in the area mainly comes from the decay of radioactive elements in the middle and upper crust, and depends on the abundance of thermogenic elements, such as ^{238}U, ^{232}Th and ^{40}K (Rybach and Buntebarth, 1984).

Previous studies have analyzed the overall heat generation rate of radioactive elements in the study area shown as low heat generation rate of strata and high heat generation rate of granitic rocks (Kuang et al., 2020). The value of heat generation rate from Yanshanian rocks is far higher than the average global continental upper crust rock, with the average value of 5.50 $\mu W/m^3$ and the maximum value up to 9.15 $\mu W/m^3$. It is also much higher than the average measured value of the radioactive heat generation rate of granitic rocks in other regions, which was about 2.5 $\mu W/m^3$ (Rybach, 1988), 3.3~3.8 $\mu W/m^3$ (Wollenberg and Smith, 1987) and 3.0 $\mu W/m^3$ (Rybach and Buntebarth, 1984).

This is mainly attributed to Yanshanian granites formed from remelting of pre-Cambian rocks in this region (Xu et al., 2007), The rocks have been experienced the redistribution process, and enriched large ion lithophile elements (LILE) of rocks, lead to extreme enrichment of LILE (including Th, U, K element), and then forming high value of heat generation rate in granites. Consequently, the high thermal conductivity and high radioactive thermogenic elements of Yanshanian granites are the reasons for the formation of high-temperature geothermal in this area.

5.4 The significance of granite to deep geothermal in southeast China

Based on produced heat rate of typical magmatic rocks in Guangdong, Jiangxi and southeast of Fujian, previous scholars indicated that the radioactive heat production rate of most granitic rocks is greater than the average heat production rate of the earth's crust, signifying that the Yanshanian granite radioactive heat production have great contribution to regional heat (Zhao et al., 1995). Meanwhile, the southeastern coastal area has basically the same tectonic evolution pattern in Mesozoic (Wang et al., 2013), which is controlled by Paleo-Pacific plate subduction during the Yanshanian period and experienced large-scale magmatic events.

Based on seismic inversion in the area, it is clear that in this area and the surrounding granite areas, based on P wave inversion of deep seismic profiles, shows 5 -10 km depth of granite. A reasonable speculation in the area is that Yashaninan granites have great potential for the geothermal reservoirs. Moreover, the Moho surface in the whole southeast region is relatively shallow and the temperature of the Moho surface is relatively high (Zhang et al., 2018). The deep granite can promote the heat transfer of the mantle to the surface. In summary, Yanshaninan granite in the southeast coastal area is of great significance to the geothermal energy system.

6. CONCLUSION

(1) The age of granites is mainly Yanshanian period, and the production background is the advance and retreat of the ancient Pacific subduction zone.

(2) Deep Yanshanian granites promote mantle heat transfer to the surface and increase the proportion of mantle heat flow in the heat flow value. Yanshanian granite has high content of Th, U and K, and its radioactive decay heat generation provides heat source for the high-temperature geothermal in the study area. The combined action of the two forms the high-temperature geothermal energy in the study area.

(3) The deep granite in the study area has huge potential for geothermal resources. The geothermal genesis model in the study area has reference significance for the understanding of geothermal in the southeast region or the calculation of geothermal reserves.

REFERENCES

Bertani, R., 2012. Geothermal Power Generation in theWorld 2005-2010 Update Report. Geothermics, 41:1-29.

Bertani, R., 2016. Geothermal Power Generation in theWorld 2010-2014 Update Report. Geothermics, 60:31-43.

Brown, D. W., Duchane, D. V., Heiken, G., et al., 2012.Mining the Earth's Heat: Hot Dry Rock Geothermal Energy. Springer Science & Business Media，Heidelberg.

Deng,Y. F., Li,J. T., Peng,T. P., et al., 2019. Lithospheric Structure in the Cathaysia Block (South China) and Its Implication for the Late Mesozoic Magmatism. Physics of the Earth and Planetary Interiors, 291: 24-34.

Frost, B. R., Barnes, C. G., Collins, W. J., et al., 2001. A Geochemical Classification for Granitic Rocks. Journalof Petrology, 42(11): 2033-2048.

Genter, A., Traineau, H., Dezayes, C., et al., 1995. Fracture Analysis and Reservoir Characterization of the Granitic Basement in the HDR Soultz Project (France). Geothermal Science & Technology, 4(3): 189-214.

Goldstein, B. A., Hill, A. J., Long, A., 2008. Hot Rocks in Australia National Overview. ASEG Extended Abstracts, (1): 1.

Gong, J. F., John Chen, Y., 2014. Evidence of Lateral Asthenosphere Flow beneath the South China Craton Driven by Both Pacific Plate Subduction and the India Eurasia Continental Collision. Terra Nova, 26(1): 55-63.

Hasterok, D., Chapman, D. S. 2007. Continental Thermal Isostasy: 2. Application to North America. Journal of Geophysical Research: Solid Earth, 112(B6).

Hu, S. B., He, L. J., Wang, J. Y., 2000. Heat Flow in the Continental Area of China: A New Data Set. Earth and Planetary Science Letters, 179(2): 407-419.

Huang, S. P., 1992. Variations of Heat Flow and Crustal Thickness in the Continental Area of China. Chinese Journal of Geophysics, 35(4): 441-450 (in Chinese with English abstract).

Kelemen, P.B., Hanghøj, K., Greene, A.R., 2003. One View of the Geochemistry of Subduction - Related Magmatic Arcs, with an Emphasis on Primitive Andesite and Lower Crust. Treatise on Geochemistry, 3: 659.

Kuang, J., Qi S., Wang, S., 2020, Granite Intrusion in Huizhou, Guangdong Province and Its Geothermal Implications, Earth Science, 45, (2020), 1466-1480.

Lackey, J. S., Valley, J., Saleeby, J., 2005. Supracrustal Input to Magmas in the Deep Crust of Sierra Nevada Batholith: Evidence from High‐δ18O Zircon. Earth and Planetary Science Letters, 235(1-2): 315-330.

Li, X. H., Li, Z. X., Li,W., et al., 2007. U– Pb Zircon, Geochemical and Sr‐Nd‐Hf Isotopic Constraints on Age and Origin of Jurassic I‐ and A‐Type Granites from Central Guangdong, SE China: A Major Igneous Event in Response to Foundering of a Subducted Flat‐Slab? Lithos, 96(1-2): 186-204.

Li, Z. X., Li, X. H., 2007. Formation of the 1 300‐km‐WideIntracontinental Orogen and Postorogenic Magmatic Province in Mesozoic South China: A Flat‐Slab Subduction Model. Geology, 35(2): 179.

Li, D. W., Wang, Y. X., 2015. Major Issues of Research and Development of Hot Dry Rock Geothermal Energy. Earth Science, 40(11):1858-1869(in Chinese with English abstract).

Liu, Y.S., Hu, Z.C., Gao, S., Günther, D., Xu, J., Gao, C.G., Chen, H.H., 2008a. In situ analysis of major and trace elements of anhydrous minerals by LA-ICP-MS without applying an internal standard. Chemical Geology, 257(1-2): 34-43.

Ludwig,K. R., 2003. Isoplot 3.00: A Geochronological Toolkit for Microsoft Excel. Berkeley Geochronology Center Special Publication, Berkeley，4, 70.

Lund, J. W., Boyd, T. L., 2016. Direct Utilization of Geothermal Energy 2015 Worldwide Review. Geothermics, 60: 66-93.

Pearce,J. A., Harris,N. B. W., Tindle, A. G., 1984. Trace Element Discrimination Diagrams for the Tectonic Interpretation of Granitic Rocks. Journal of Petrology, 25(4): 956-983.

Richards,H. G., Savage, D., Andrews, J. N., 1992. Granite‐ Water Reactions in an Experimental Hot Dry Rock Geothermal Reservoir, Rose-manowes Test Site, Cornwall, U. K. Applied Geochemistry, 7(3): 193-222.

Rudnick,R. L., Fountain, D. M., 1995. Nature and Composition of the Continental Crust: A Lower Crustal Perspective. Reviews of Geophysics, 33(3): 267.

Rybach, L., Buntebarth, G., 1984. The Variation of Heat Generation, Density and Seismic Velocity with Rock Type in the Continental Lithosphere. Tectonophysics, 103(1-4): 335-344.

Rybach, L., 1988. Determination of Heat Production Rate. Handbook of Terrestrial Heat Flow Density Determinations.

Sclater,J. G., Jaupart, C., Galson, D., 1980. The Heat Flow through Oceanic and Continental Crust and the Heat Loss of the Earth. Reviews of Geophysics, 18(1): 269- 311.

Sun,S. S., McDonough,W. F., 1989. Chemical and Isotopic Systematics of Oceanic Basalts: Implications for Mantle Composition and Processes. Geological Society, London, Special Publications, 42(1): 313-345.

Tan, H., Lin F., Wen, J., Li, J., Fan, Y., Application of wide field electromagnetic method in the exploration of deep dry hot rocks in Hainan province. 2020, China Petroleum and Chemical Standard and Quality, (4) 150-152. (in Chinese with English abstract)

Wang,Y. J., Fan,W. M., Zhang,G. W., et al., 2013. Phanerozoic Tectonics of the South China Block: Key Observations and Controversies. Gondwana Research, 23(4):1273-1305.

Wang, S.J., Hu, S.B., Wang, S.J., et al., 1999.The Geothermal Effect of Radioactive Heat Generation and Its Signif‐icance to Hydrocarbon Maturation in Tarim Basin. Petroleum Exploration and Development, 26(5): 36-38, 5 (in Chinese with English abstract).

Wollenberg, H. A., Smith, A. R., 1987. Radiogenic Heat Production of Crustal Rocks: An Assessment Based on Geochemical Data. Geophysical Research Letters, 14(3): 295-298.

Xi, Y. F., Wang, G. L., Liu, S., et al., 2018. The Formation of a Geothermal Anomaly and Extensional Structures in Guangdong, China: Evidence from Gravity Analyses. Geothermics, 72: 225-231.

Xu, X. S., O'Reilly, S. Y., Griffin, W. L., et al., 2007. The Crust of Cathaysia: Age, Assembly and Reworking of Two Terranes. Precambrian Research, 158(1-2): 51-78.

Yuan, Y. S., Ma, Y. S., Hu, S. B., et al., 2006. Present‐Day Geothermal Characteristics in South China. Chinese Journal of Geophysics, 49(4): 1118-1126(in Chinese with English abstract).

Zhang, J., Wang, B.Y., Tang, X.C., et al.,2018. Temperature Structure and Dynamic Background of Crust and Mantle

beneath the High Heat Flow Area of the South China Continental Margin. Chinese Journal of Geophysics, 61(10):3917-3932(in Chinese with English abstract).

Zhao, P., Wang, J., Wang, J.A.,et al., 1995. Characteristics of Heat Production Distribution in SE China. Acta Petrologica Sinica, 11(3), 292-305 (in Chinese with English abstract).

Zhou, X. M., Sun,T., Shen,W. Z., et al., 2006. Petrogenesis of Mesozoic Granitoids and Volcanic Rocks in South China: A Response to Tectonic Evolution. Episodes, 29(1): 26-33.